Supplementary Information

Spectral and photophysical modifications of porphyrins attached to core-shell nanoparticles. Theory and experiment

Keywords: porphyrin, core-shell nanoparticles, plasmonics, fluorescence

Submitted to: *Methods Appl. Fluoresc.*

1. Synthesis

1.1. Meso-tetraphenyl porphyrin and its zinc(II) complex

Meso-tetraphenylporphyrin (TPP) was synthesized and purified according to Rothemund procedure [1]. ^{1}H NMR (400 MHz, $CDCl_3$) δ 8.86 (bs, 8H), 8.27 - 8.20 (m, 8H), 7.82 – 7.70 (m, 12H), -2.75 (s, 2H). ^{13}C NMR (400 MHz, $CDCl_3$) δ 142.16, 134.54, 127.69, 126.66, 120.12.

The tetraphenylporphyrin zinc complex ZnTPP was synthesized by reaction of TPP and $Zn(OAc)_2$ in MeOH/THF mixture according to the literature procedure [2]. ^{1}H NMR (400 MHz, $CDCl_3$) δ 8.96 (bs, 8H), 8.27 - 8.20 (m, 8H), 7.81 – 7.71 (m, 12H). ^{13}C NMR (400 MHz, $CDCl_3$) δ 150.21, 142.78, 134.41, 127.49, 126.54, 121.15.

TPP [3] and ZnTPP [2] NMR spectra agree with the respective literature data.

1.2. Synthesis of silica-coated gold nanoparticles

Silica-coated gold nanoparticles (gold cores: 39, 49, and 64 nm in radius, and silica thickness: 18, 17, and 15 nm, respectively) were synthesized by a modified protocol developed by Liz-Marzán [4]. Gold nanospheres were prepared by the well-known seeded growth process in the presence of a cationic surfactant hexadecyltrimethylammonium bromide (CTAB) and using ascorbic acid as a mild reducing agent. Subsequently the gold nanoparticles were functionalized with thiolated poly(ethylene glycol) (PEG-SH, Mw: 5 K). Upon PEG stabilization, the gold nanoparticles were transferred to ethanol, where silica can be grown on the nanoparticles surface following the well-established Stöber method. To control the thickness of the silica layer for each particle diameter (39, 49, and 64 nm), during the coating process the concentration of nanoparticles in terms of metallic gold, [Au^0], was 1.6, 1.2, and 1.5 mM, respectively.

PEG-coated and silica-coated nanoparticles were characterized with a scanning electron microscopy (SEM) to provide the statistics of gold core diameter and silica shell thickness distributions.

1.2.1. Synthesis of porphyrin amino derivative

4-(3-hydroxy-1-propyn-1-yl)-benzaldehyde, S1: Compound S1 was synthesized according to the previously reported protocol [5]. ^{1}H NMR (500 MHz; $CDCl_3$): 10.00 (s, 1H), 7.83 (d, J= 8.22 Hz, 2H), 7.58 (d, J = 8.22 Hz, 2H), 4.54 (s, 2H), 1.85 (br, s, 1H).

4-(3-acetoxy-1-propyn-1-yl)-benzaldehyde, S2: Aldehyde S1 (4.69 g, 29.3 mmol) was dissolved in CH_2Cl_2 (250 mL). Then acetic acid anhydride was added (5.53 mL, 58.5 mmol), followed by the addition of triethylamine (20 mL, 143.6 mmol). The reaction progress was monitored by TLC (ethyl acetate: hexanes 1:2). After the reaction was completed, solvent was evaporated and the product was isolated by column

chromatography (SiO_2, ethyl acetate: hexanes 1:4) as a pale yellow solid. ^{1}H NMR (400 MHz; $CDCl_3$) δ 10.00 (s, 1H), 7.83 (d, 2H, J = 8.1 Hz), 7.59 (d, 2H, J = 8.1 Hz), 4.92 (s, 2H), 2.14 (s, 2H). ^{13}C NMR (400 MHz; $CDCl_3$) δ 191.2, 170.37, 135.79, 132.36, 129.49, 128.30, 87.22, 85.11. HR-MS (ESI+) m/z $[M+H]^+$ 202.0623, calcd for $C_{12}H_{10}O_3$ 202.0630.

5-[4-(3-hydroxy-1-propyn-1-yl)phenyl]-10,15,20-triphenylporphyrin, S3: Aldehyde S2 (2.00 g, 9.99 mmol), benzaldehyde (3 mL, 29.72 mmol) and pyrrole (2.75 mL, 39.70 mmol), were dissolved in chloroform (1900 mL). Next, trifluoroboron etherate (1.59 mL, 12.87 mmol) was added and the mixture was stirred at room temperature for 2 h. Then the triethylamine (1.87 mL, 13.60 mmol) was added. The mixture was stirred for 5 min and chloranil was added (7.3 g, 29.7 mmol). After 20 min the solution was removed, the dry residue was dissolved in CH_2Cl_2 (100 mL) and filtered through the silica pad. During the filtration, the product is eluted as a second fraction and may be partially separated from tetraphenylporphyrin (first fraction) and multiply substituted porphyrin. The filtrate containing second fraction was collected and the solvent was removed. The obtained material was dissolved in THF/MeOH mixture (v/v 10:1, 200 mL) and NaOH (800 mg, 20 mmol). The hydrolysis was monitored by TLC. When the hydrolysis was completed, the mixture was subjected to the standard work-up. The porphyrin S3 was isolated by column chromatography (SiO_2, $HCCl_3$) as a second fraction preceded by nonpolar fraction containing tetraphenylporphyrin. The porphyrin was obtained with the yield of 12.7% (848 mg, 1.27 mmol). ^{1}H NMR (400 MHz, $CDCl_3$) δ 8.9 – 8.81 (m, 8H), 8.26 – 8.16 (m, 8H), 7.86 – 7.72 (m, 11H), 4.65 (s, 2H), -2.76 (s, 2H). ^{13}C NMR (400 MHz, $CDCl_3$) δ 142.57, 142.07, 134.53, 134.50, 130.04, 127.74, 126.69, 122.01, 120.39, 120.28, 118.99, 88.33, 85.74, 51.84. HR-MS (ESI+) m/z $[M+H]^+$ 669.2678, calcd for $C_{47}H_{32}N_4O^+$ 669.2654.

5-[4-(3-bromo-1-propyn-1-yl)phenyl]-10,15,20-triphenylporphyrin, S4: Porphyrin S3 (660 mg, 0.98 mmol), tetrabromomethane (654 mg, 1.97 mmol) and triphenylphosphine (520 mg, 1.98 mmol), were dissolved in CH_2Cl_2 (300 mL). The mixture was stirred for 30 min. After that time, the solvent was removed and the porphyrin was isolated by column chromatography (SiO_2, CH_2Cl_2: hexanes 1:2). The product was obtained with 69% yield (499 mg, 0.68 mmol). ^{1}H NMR (400 MHz, $CDCl_3$) δ 8.99 – 8.75 (m, 8H), 8.31 – 8.12 (m, 8H), 7.90 – 7.69 (m, 11H), 4.33 (s, 2H), -2.75 (s, 2H). ^{13}C NMR (101 MHz, $CDCl_3$) δ 142.98, 142.13, 134.57, 130.30, 127.79, 126.73, 121.48, 120.48, 120.35, 118.91, 87.47, 82.20, 40.80. HR-MS (ESI+) m/z $[M+H]^+$ 731.1818, calcd for $C_{47}H_{32}N_4Br^+$ 731.1810.

5-[4-(3-amino-1-propyn-1-yl)phenyl]-10,15,20-triphenylporphyrin, S5: A Schlenk tube was charged with liquid NH_3 (2-3 mL), anhydrous THF (30 mL) and porphyrin S4 (62 mg, 0.08 mmol), at -78 °C under argon atmosphere. The reaction mixture was allowed to reach room temperature and was stirred overnight.

After evaporation, the crude product was purified by column chromatography (SiO_2, CH_2Cl_2 : methanol 10:1). The product was obtained with 40% yield (0.23 mg, 0.0324 mmol) ^{1}H NMR (400 MHz, $CDCl_3$) δ 9.01 – 8.86 (m, 8H), 8.35 – 8.19 (m, 8H), 7.89 – 7.74 (m, 11H), 3.85 (s, 2H), -2.66 (s, 2H). ^{13}C NMR (101 MHz, $CDCl_3$) δ 142.17, 142.11, 134.60, 134.55, 131.37, 129.98, 127.80, 126.75, 122.80, 120.44, 120.35, 119.27, 91.53, 82.52, 32.45. HR-MS (EI+) m/z $[M]^+$ 668.2791, calcd for $C_{47}H_{34}N_5^+$ 668.2814.

1.2.2. Functionalization of silica-coated gold nanoparticles with porphyrin The concentrations were fixed to maintain the ratios [porphyrin] / [nm^2] = 20-35 molecules / nm^2 and [linker] / [porphyrin] = 3. The silica-coated nanoparticles were transferred to the anhydrous DMF solution via centrifugation-redispersion procedure repeated at least 3 times. The final volume of such obtained Au@SiO_2 nanoparticles suspension was approximately 5 mL. The concentration of [Au^0] was maintained at [Au^0] = 1.5 mM by addition of DMF. The Au@SiO_2 nanoparticles solution was then transferred to the round bottom flask and kept under N_2 atmosphere. Porphyrin (1.50 mg, 2.0 μmol) solution in anhydrous DMF (200 µl) was prepared in a separate vial. Then 3-(triethoxysilyl)propyl isocyanate (1.5 mg, 0.6 μmol) was added. The vial was closed with Teflon cap and the mixture was stirred for 1 h at 50^{o}C. After that time, a portion of 12 μl of porphyrin solution was added to the solution of the nanoparticles to provide 20-35 porphyrin molecules per nm^2 of the Au@SiO_2 nanoparticles surface. Then the solution of the nanoparticles was stirred at 90^{o}C overnight. Finally, the obtained functionalized nanoparticles were purified via centrifugation-redispersion proce dure (15 min; 2000 rpm for 130 and 100 nm gold cores and 4000 rpm for 80 nm gold core) using DMF.

1.2.3. Functionalization of silica nanoparticles with porphyrin The concentrations were fixed to maintain the rations [porphyrin] / [nm^2] = 20 molecules / nm^2 and [linker] / [porphyrin] = 20. The reaction was carried out under the argon atmosphere. To the solution of porphyrin S5 (4.21 mg, 6.3 μmol) in anhydrous THF (0.5 mL) and anhydrous DMF (2 mL) 3-(triethoxysilyl)propyl isocyanate (29.3 μL, 118.45 μmol) and SiO_2 nanoparticles (stock solution, 100 μL, 10% v/v in ethanol, diameter =140 nm, Sigma-Aldrich) were added. The mixture was then heated to 80^{o}C and stirred at this temperature overnight. After that time, the mixture was centrifuged (10000 rpm, 15 min) and redispersed in THF (4 mL) 5 times. The nanoparticles were then transferred to DMF via centrifugation-redispersion procedure.

1.3. Complexing SiO_2-H_2TPP and Au@SiO_2-H_2TPP with Zn

A zinc complex of TPP attached to nanoparticles was obtained by applying zinc acetate dihydrate (ACS reagent, Sigma Aldrich) to the nanoparticles with free-base TPP on their surface. The suspension was left overnight. The nanoparticles were purified via centrifugation-redispersion procedure (15 min; 2000 rpm for 130 and 100 nm gold cores,

4000 rpm for 80 nm gold core, and 10000 rpm for SiO_2 nanoparticles) using DMF.

2. Kinetics of the photophysics in the steady-state approximation in the numerical simulations

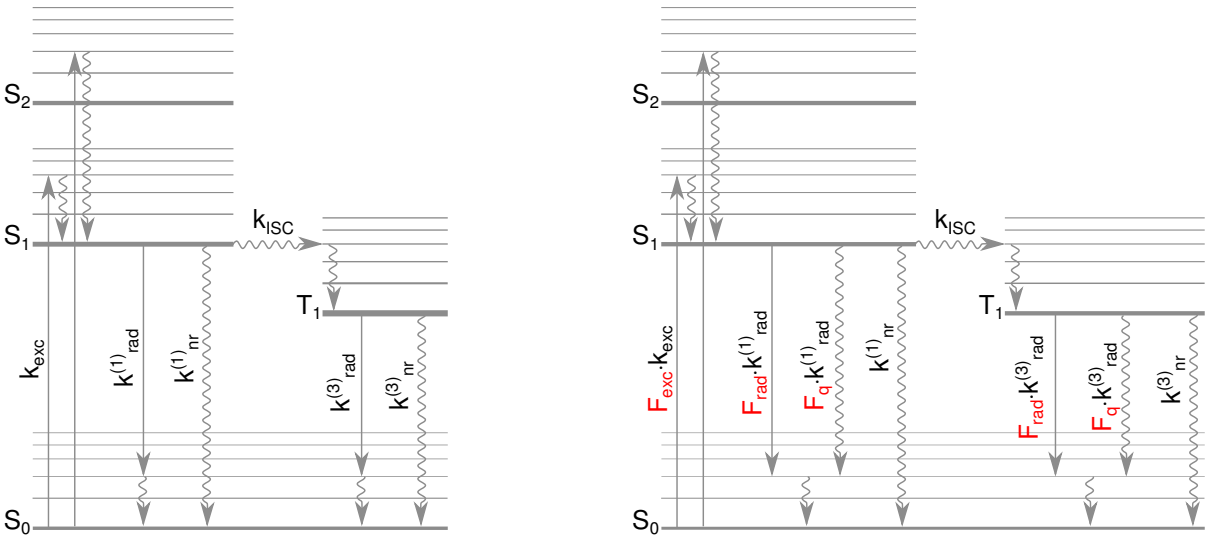

(a) Without the metal nanoparticle in the system.

(b) In the presence of the metal nanoparticle in the system.

Figure S1: Jabłoński diagrams depicting changes in radiative rates introduced by the presence of a metal nanoparticle.

Figure S1a depicts the Jabłoński diagram with electronic levels and vibronic transitions of the chromophore. Radiative transitions (solid line) correspond to absorption, emission from the singlet excited state (fluorescence) and emission from the triplet state (phosphorescence). The rate constants for these processes are labeled k_{exc}, $k_{rad}^{(1)}$ and $k_{rad}^{(3)}$, respectively.

Figure S1b depicts analogous diagram for a chromophore in the regime of weak-coupling with a plasmonic nanostructure. Only radiative transitions have been modified by the interaction. Additionally, part of the excited state emission is absorbed by the nanostructure ($F_q \cdot k_{rad}$).

All of the rate constants k and enhancement factors F (defined in figure S1b) are wavelength-dependent, therefore the kinetics in figure S1 is presented in terms of integrals over the emission bands or excitation light. The notation used is as follows:

$$k = \int k(\lambda) \cdot d\lambda \tag{S1}$$

and

$$F \cdot k = \int F(\lambda) \cdot k(\lambda) \cdot d\lambda, \tag{S2}$$

which results in:

$$F = \frac{\int F(\lambda) \cdot k(\lambda) \cdot d\lambda}{k} \tag{S3}$$

defining all F_{exc}, F_{rad} and F_{tot} used in formulae below.

Kinetics of the interaction of plasmons with light in the spherical nanoparticle are about 6 orders of magnitude faster than the analogous processes in the chromophore. Therefore they can be considered as infinitely fast which rationalizes the use the stationary state approximation [6], which is often employed for similar systems. The main assumption in this model is the constant concentration of molecules in each of the excited states. Adopting subscript g for the ground state and s, t for the excited singlet and triplet states, respectively, this assumption can be expressed as:

$$\begin{aligned}\frac{dN_s}{dt} &= \\ &= F_{exc}\cdot k_{exc}\cdot N_g - (F_{rad}^{(1)}\cdot k_{rad}^{(1)} + F_q^{(1)}\cdot k_{rad}^{(1)} + k_{ISC} + k_{nr}^{(1)})\cdot N_s \approx 0\end{aligned} \tag{S4}$$

$$\frac{dN_t}{dt} = k_{ISC}\cdot N_s - (F_{rad}^{(3)}\cdot k_{rad}^{(3)} + F_q^{(3)}\cdot k_{rad}^{(3)} + k_{nr}^{(3)})\cdot N_t \approx 0 \tag{S5}$$

Additionally,

$$N = N_g + N_s + N_t. \tag{S6}$$

The above equations can provide the fraction of molecules in the excited singlet and triplet states:

$$N_s = N\cdot \cdot\frac{F_{exc}\cdot k_{exc}\cdot (F_{tot}^{(3)}\cdot k_{rad}^{(3)} + k_{nr}^{(3)})}{(F_{tot}^{(1)}\cdot k_{rad}^{(1)} + k_{nr}^{(1)} + k_{ISC})\cdot (F_{tot}^{(3)}\cdot k_{rad}^{(3)} + k_{nr}^{(3)}) + F_{exc}\cdot k_{exc}\cdot (F_{tot}^{(3)}\cdot k_{rad}^{(3)} + k_{nr}^{(3)} + k_{ISC})} \tag{S7}$$

and

$$N_t = N\cdot \cdot\frac{F_{exc}\cdot k_{exc}\cdot k_{ISC}}{(F_{tot}^{(1)}\cdot k_{rad}^{(1)} + k_{nr}^{(1)} + k_{ISC})\cdot (F_{tot}^{(3)}\cdot k_{rad}^{(3)} + k_{nr}^{(3)}) + F_{exc}\cdot k_{exc}\cdot (F_{tot}^{(3)}\cdot k_{rad}^{(3)} + k_{nr}^{(3)} + k_{ISC})}, \tag{S8}$$

where $F_{tot}^{(1)} = F_{rad}^{(1)} + F_q^{(1)}$ and $F_{tot}^{(3)} = F_{rad}^{(3)} + F_q^{(3)}$.

In the case of weak excitation light intensity:

$$(F_{tot}^{(1)}\cdot k_{rad}^{(1)} + k_{nr}^{(1)} + k_{ISC})\cdot (F_{tot}^{(3)}\cdot k_{rad}^{(3)} + k_{nr}^{(3)}) >> F_{exc}\cdot k_{exc}\cdot (F_{tot}^{(3)}\cdot k_{rad}^{(3)} + k_{nr}^{(3)} + k_{ISC})$$

For porphyrins, the term on the left is about 3 orders of magnitude larger. Therefore, the formulae can be. approximated as:

$$N_s \approx N\cdot \frac{F_{exc}\cdot k_{exc}}{F_{tot}^{(1)}\cdot k_{rad}^{(1)} + k_{nr}^{(1)} + k_{ISC}} \tag{S9}$$

$$N_t \approx N\cdot \frac{F_{exc}\cdot k_{exc}\cdot k_{ISC}}{(F_{tot}^{(1)}\cdot k_{rad}^{(1)} + k_{nr}^{(1)} + k_{ISC})\cdot (F_{tot}^{(3)}\cdot k_{rad}^{(3)} + k_{nr}^{(3)})} \tag{S10}$$

The relative changes of the excited state lifetimes are equal to:

$$F_\tau^{(1)} = \frac{\tau^{(1)}}{\tau_0^{(1)}} = \frac{1}{\tau_0^{(1)}}\cdot \frac{1}{F_{tot}^{(1)}\cdot k_{rad}^{(1)} + k_{nr}^{(1)} + k_{ISC}} \tag{S11}$$

and

$$F_{\tau}^{(3)} = \frac{\tau^{(3)}}{\tau_0^{(3)}} = \frac{1}{\tau_0^{(3)}} \cdot \frac{1}{F_{tot}^{(3)} \cdot k_{rad}^{(3)} + k_{nr}^{(3)}} \tag{S12}$$

which simplifies the formulae for excited states populations to:

$$N_s = N \cdot F_{exc} \cdot k_{exc} \cdot F_{\tau}^{(1)} \cdot \tau_0^{(1)} \tag{S13}$$

$$N_t = N \cdot F_{exc} \cdot k_{exc} \cdot k_{ISC} \cdot F_{\tau}^{(1)} \cdot \tau_0^{(1)} \cdot F_{\tau}^{(3)} \cdot \tau_0^{(3)} \tag{S14}$$

At the same time, the emission intensity is expressed as:

$$\begin{aligned} &\Gamma_{rad}^{(1)}(\lambda) = N_s \cdot F_{rad}^{(1)}(\lambda) \cdot k_{rad}^{(1)}(\lambda) = \\ &= F_{rad}^{(1)}(\lambda) \cdot k_{rad}^{(1)}(\lambda) \cdot N \cdot F_{exc} \cdot k_{exc} \cdot F_{\tau}^{(1)} \cdot \tau_0^{(1)} \end{aligned} \tag{S15}$$

$$\begin{aligned} &\Gamma_{rad}^{(3)}(\lambda) = N_t \cdot F_{rad}^{(3)}(\lambda) \cdot k_{rad}^{(3)}(\lambda) = \\ &= F_{rad}^{(3)}(\lambda) \cdot k_{rad}^{(3)}(\lambda) \cdot N \cdot F_{exc} \cdot k_{exc} \cdot k_{ISC} \cdot F_{\tau}^{(1)} \cdot \tau_0^{(1)} \cdot F_{\tau}^{(3)} \cdot \tau_0^{(3)} \end{aligned} \tag{S16}$$

or, after integrating the rates over the emission band:

$$\Gamma_{rad}^{(1)} = F_{rad}^{(1)} \cdot k_{rad}^{(1)} \cdot N \cdot F_{exc} \cdot k_{exc} \cdot F_{\tau}^{(1)} \cdot \tau_0^{(1)} \tag{S17}$$

$$\Gamma_{rad}^{(3)} = F_{rad}^{(3)} \cdot k_{rad}^{(3)} \cdot N \cdot F_{exc} \cdot k_{exc} \cdot k_{ISC} \cdot F_{\tau}^{(1)} \cdot \tau_0^{(1)} \cdot F_{\tau}^{(3)} \cdot \tau_0^{(3)}. \tag{S18}$$

Thus, the enhancement of the emission brightness is expressed as:

$$F_{\Gamma_{rad}^{(1)}} = F_{rad}^{(1)} \cdot F_{exc} \cdot F_{\tau}^{(1)} \tag{S19}$$

$$F_{\Gamma_{rad}^{(3)}} = F_{rad}^{(3)} \cdot F_{exc} \cdot F_{\tau}^{(1)} \cdot F_{\tau}^{(3)}. \tag{S20}$$

2.1. Enhancement of the singlet oxygen generation rate

Singlet oxygen generation efficiency equals [7]:

$$\Phi_{\Delta,0} = \phi_t \cdot \frac{k_{ET} \cdot [O_2]}{k_{rad}^{(3)} + k_{nr}^{(3)} + k_q \cdot [O_2]} \tag{S21}$$

where ϕ_t is the triplet state formation quantum yield, k_{ET} is the energy transfer rate between the triplet chromophore and the oxygen molecule, leading to singlet oxygen, k_q is the triplet quenching rate by the oxygen (it includes k_{ET}). Equation S21 can be rewritten as:

$$\Phi_{\Delta,0} = k_{ISC} \cdot \tau_0^{(1)} \cdot \frac{k_{ET} \cdot [O_2]}{k_{rad}^{(3)} + k_{nr}^{(3)} + k_q \cdot [O_2]} \tag{S22}$$

In the presence of a gold nanoparticle, not only will the radiative decay rates be modified resulting in the observed modification in the singlet oxygen formation yield, but also the excitation rate.

Singlet oxygen directly after the energy transfer in the $b\ ^1\Sigma_g^+$ state, then it decays to $a\ ^1\Delta_g$ state, which is commonly referred to as *singlet oxygen* [7]. This transition is both

radiative $k_{rad}^{b\to a} \approx 10^4\ s^{-1}$ and non-radiative $k_{nr}^{b\to a} \approx 10^7\ s^{-1}$ [8]. Because $k_{rad}^{b} \ll k_{nr}^{b}$, nanoparticle will have a negligible effect on the $b \to a$ transition rate.

Therefore, in the presence of a nanoparticle:

$$\Phi_\Delta = k_{ISC} \cdot F_\tau^{(1)} \cdot \tau_0^{(1)} \cdot \frac{k_{ET} \cdot [O_2]}{F_{tot}^{(3)} \cdot k_{rad}^{(3)} + k_{nr}^{(3)} + k_q \cdot [O_2]} \tag{S23}$$

Assuming negligible influence of the nanoparticle on the triplet lifetime in the presence of oxygen, $F_{tot}^{(3)} \cdot k_{rad}^{(3)} + k_{nr}^{(3)} \ll k_q \cdot [O_2]$:

$$\Phi_\Delta \approx k_{ISC} \cdot F_\tau^{(1)} \cdot \tau_0^{(1)} \cdot \frac{k_{ET}}{k_q} \tag{S24}$$

$$F_{\Phi_\Delta} = F_\tau^{(1)} \tag{S25}$$

which is the enhancement of the $a\ ^1\Delta_g$ population formation efficiency, equal to S_1 state population enhancement. The total enhancement in the $a\ ^1\Delta_g$ formation rate will include also enhancement of excitation to S_1, F_{exc}:

$$F_{k_\Delta} = F_{exc} \cdot F_\tau^{(1)} \tag{S26}$$

Comparing equation S26 to equation S9, it is apparent that F_{k_Δ} is equivalent to the enhancement of S_1 population, F_{S_1}. Moreover, under the above assumption of negligible modifications of triplet lifetime, $F_\tau^{(3)}$, it is also equal to the enhancement of T_1 population, F_{T_1} (equation S10.)

3. Results of the simulations

Below are presented the results for simulations of the photophysical properties of H_2TPP and ZnTPP attached to $Au@SiO_2$ nanoparticle outer surface. Distance of the chromophore center to the nanoparticle surface is 2 nm.

3.1. Excitation enhancement

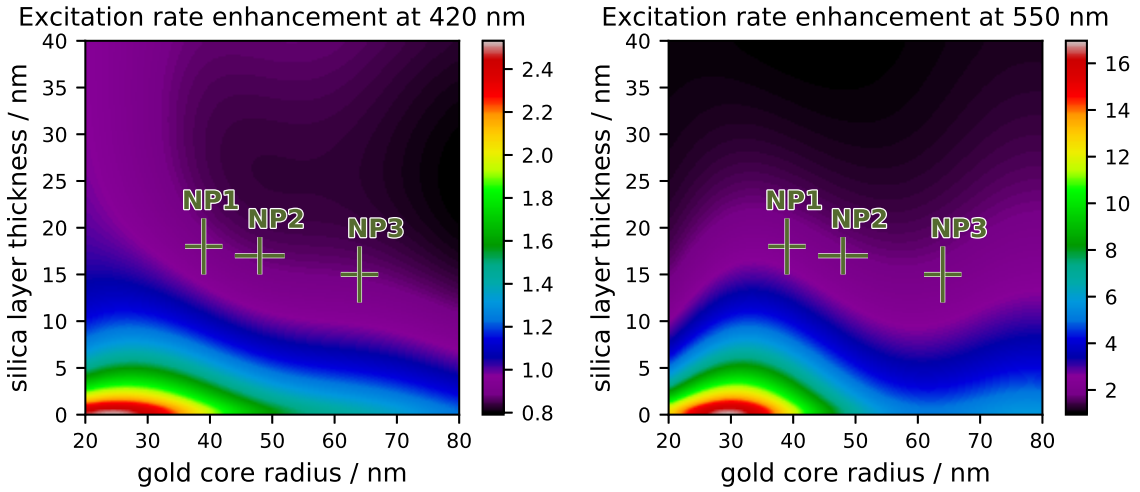

Figure S2: Simulated enhancement of excitation at 420 nm (left) and 550 nm for system with various gold core radii and silica shell thicknesses.

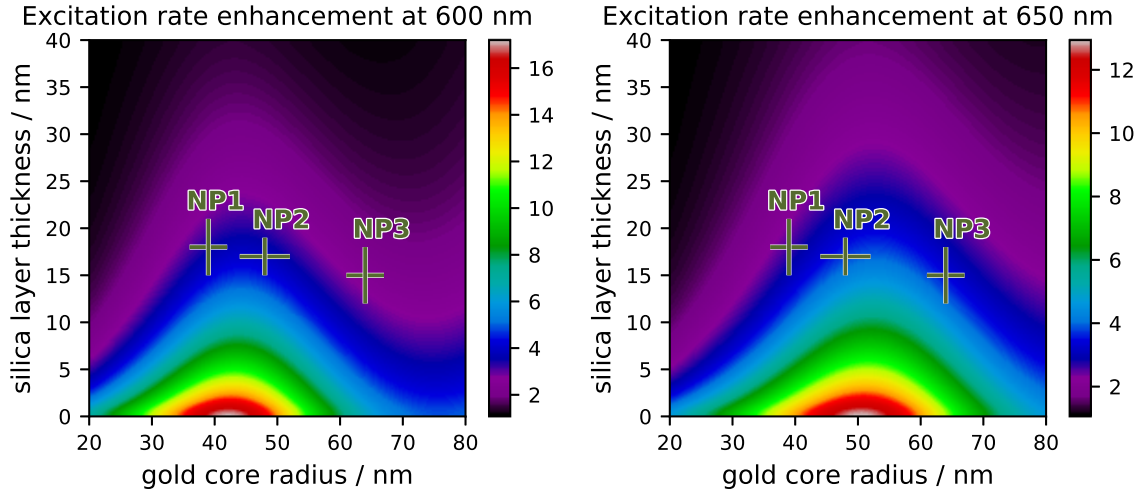

Figure S3: Simulated enhancement of excitation at 600 nm (left) and 650 nm for system with various gold core radii and silica shell thicknesses.

3.2. Radiative decay rate enhancement

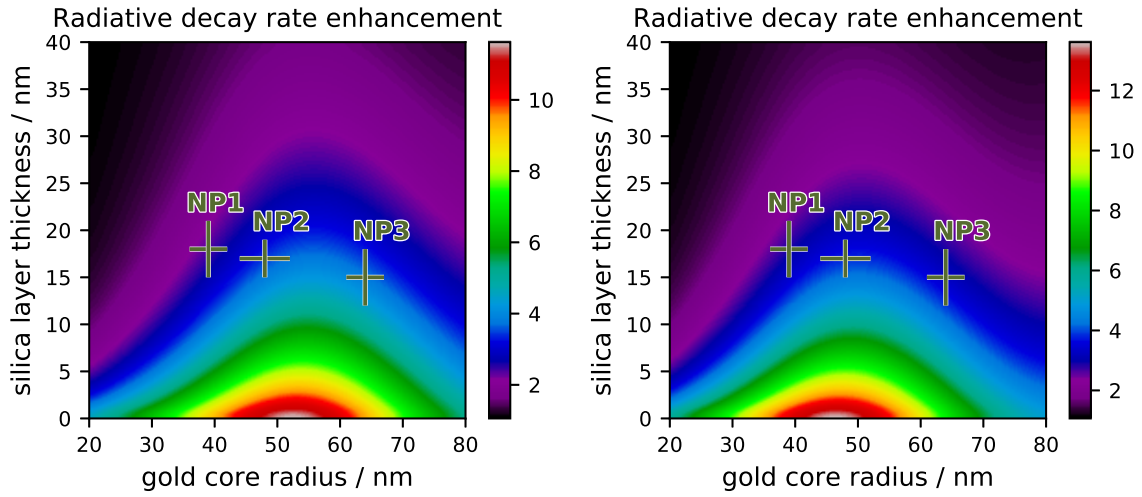

Figure S4: Simulated enhancement of the S_1 state radiative decay rate for H_2TPP (left) and ZnTPP (right) attached to Au@SiO_2 nanoparticles of different core radii and silica shell thicknesses averaged over their respective emission spectra.

3.3. S_1 state lifetime reduction

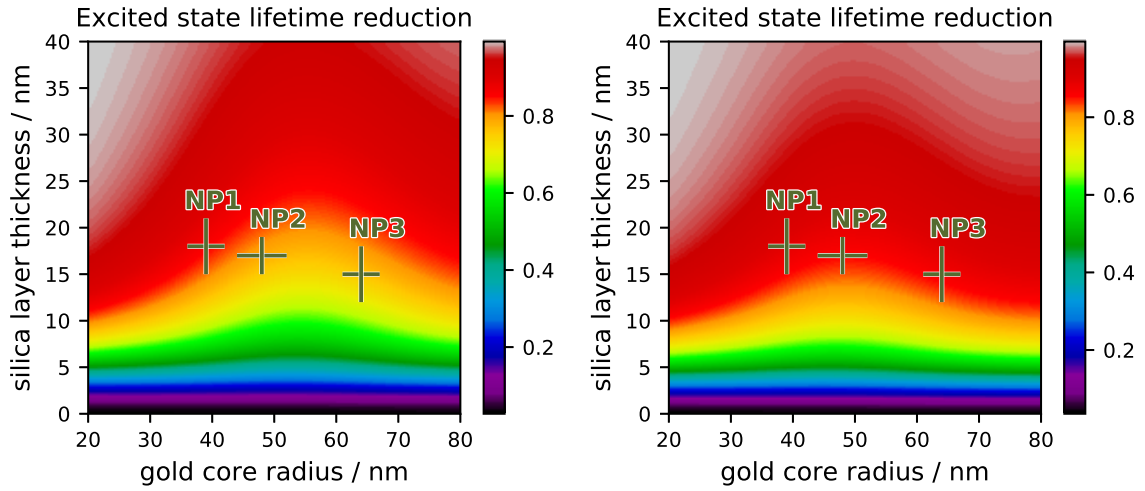

Figure S5: S_1 state lifetime reduction for H_2TPP (left) and ZnTPP (right) attached to Au@SiO_2 nanoparticles of different core radii and silica shell thicknesses averaged over their respective emission spectra.

3.4. Quantum yield enhancement

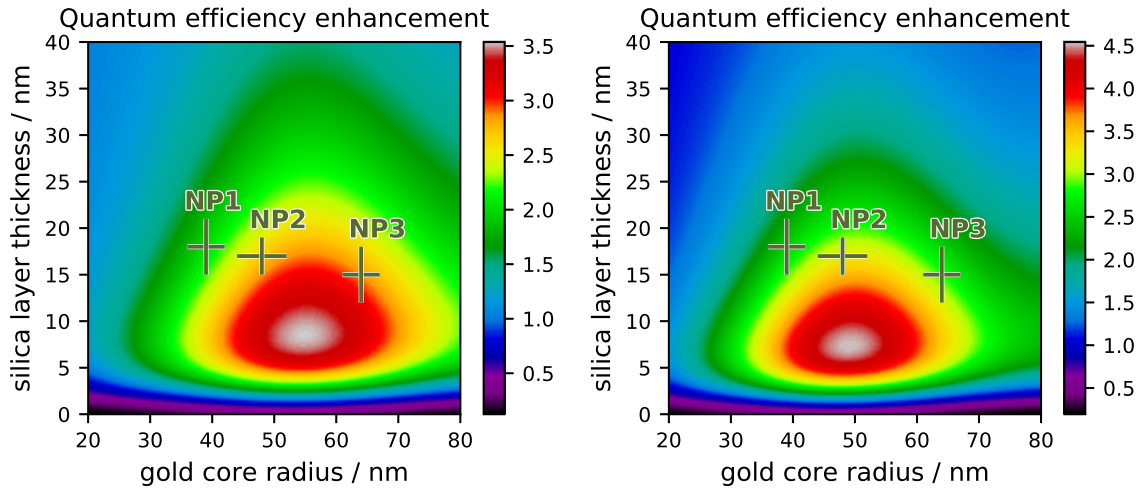

Figure S6: Simulated enhancement of quantum yield of S_1 state emission for H_2TPP (left) and ZnTPP (right) attached to Au@SiO_2 nanoparticles of different core radii and silica shell thicknesses averaged over their respective emission spectra.

3.5. S_1 state population enhancement

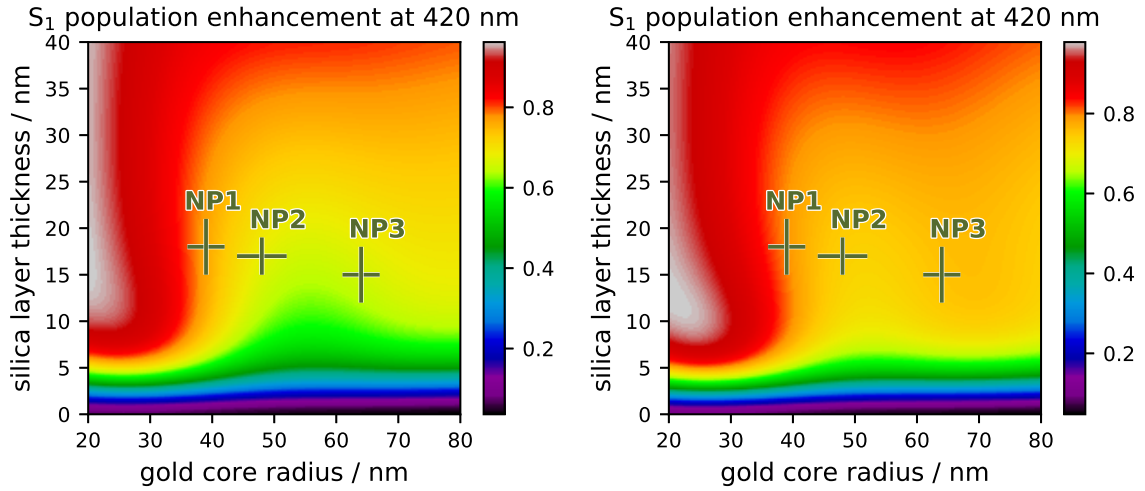

Figure S7: Simulated enhancement of the S_1 state population for H_2TPP (left) and ZnTPP (right) excited at 420 nm attached to Au@SiO_2 nanoparticles of different core radii and silica shell thicknesses.

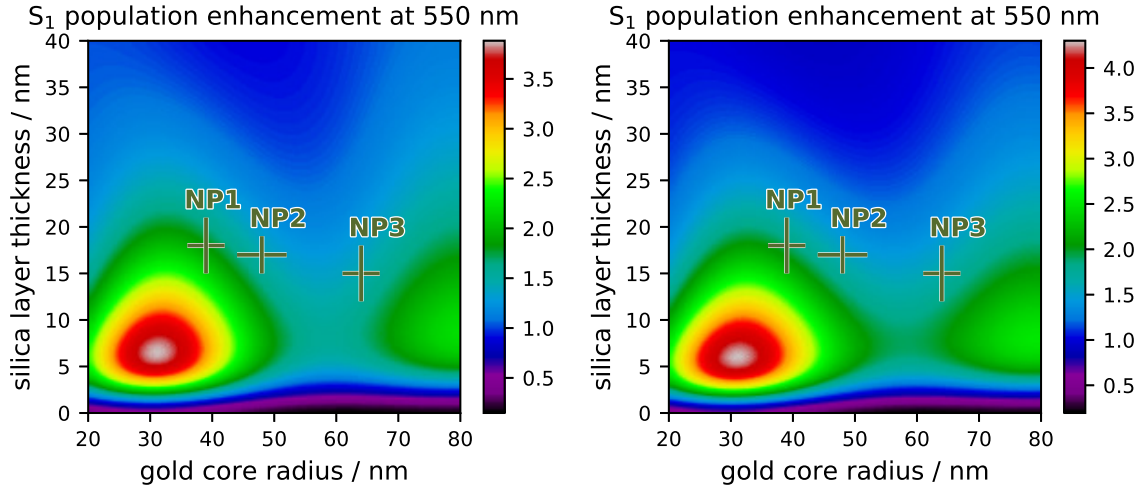

Figure S8: Simulated enhancement of the S_1 state population for H_2TPP (left) and ZnTPP (right) excited at 550 nm attached to Au@SiO_2 nanoparticles of different core radii and silica shell thicknesses .

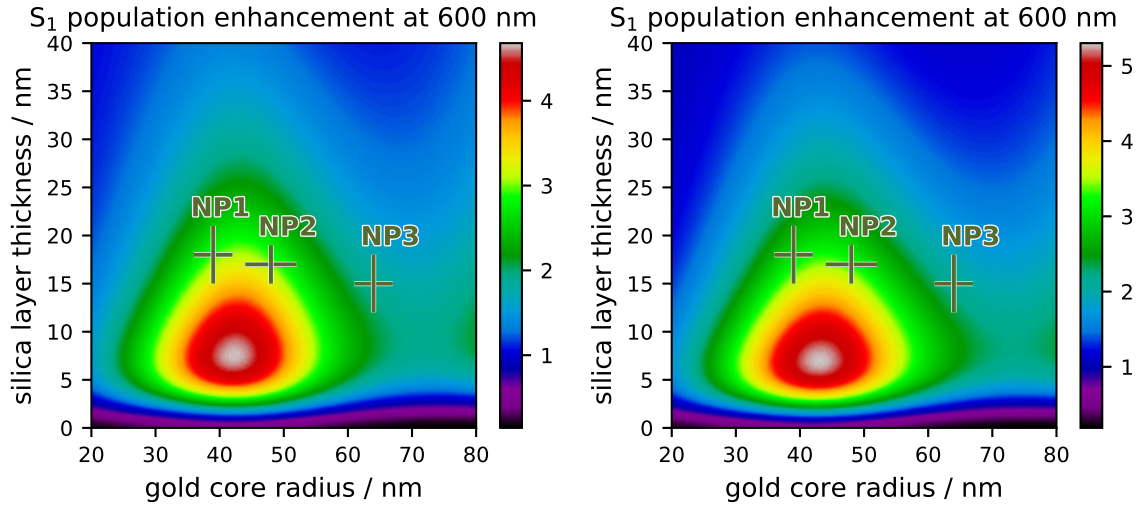

Figure S9: Simulated enhancement of the S_1 state population for H_2TPP (left) and ZnTPP (right) excited at 600 nm attached to Au@SiO_2 nanoparticles of different core radii and silica shell thicknesses.

3.6. Apparent brightness of the molecule emission

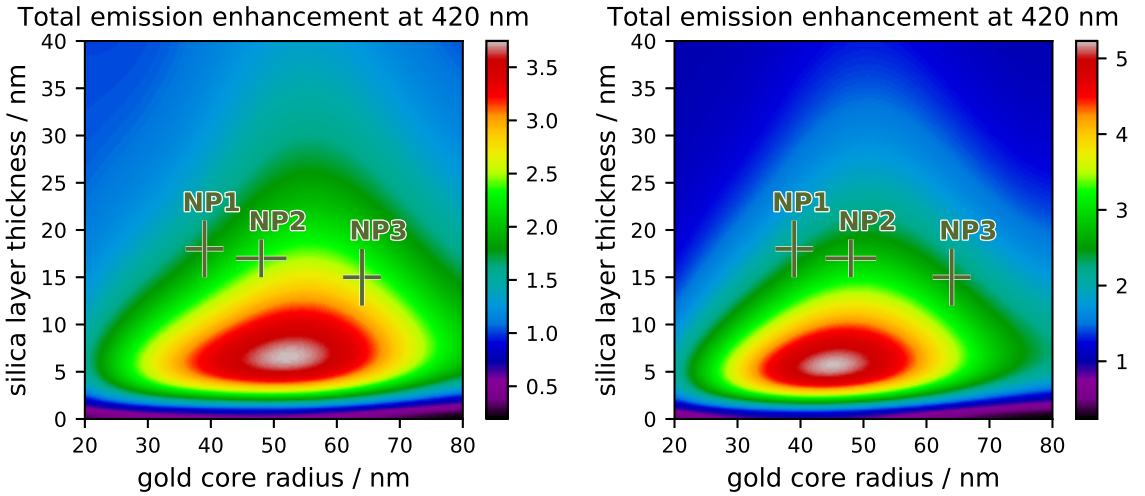

Figure S10: Simulated enhancement of the apparent brightness of the S_1 state emission for H_2TPP (left) and ZnTPP (right) excited at 420 nm attached to Au@SiO_2 nanoparticles of different core radii and silica shell thicknesses averaged over their respective emission spectra.

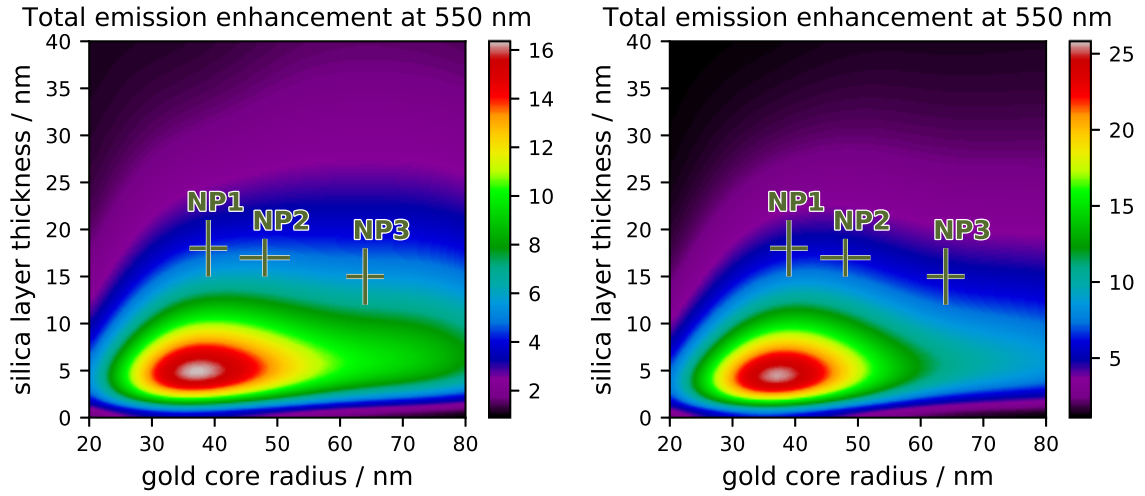

Figure S11: Simulated enhancement of the apparent brightness of the S_1 state emission for H_2TPP (left) and ZnTPP (right) excited at 550 nm attached to Au@SiO_2 nanoparticles of different core radii and silica shell thicknesses averaged over their respective emission spectra.

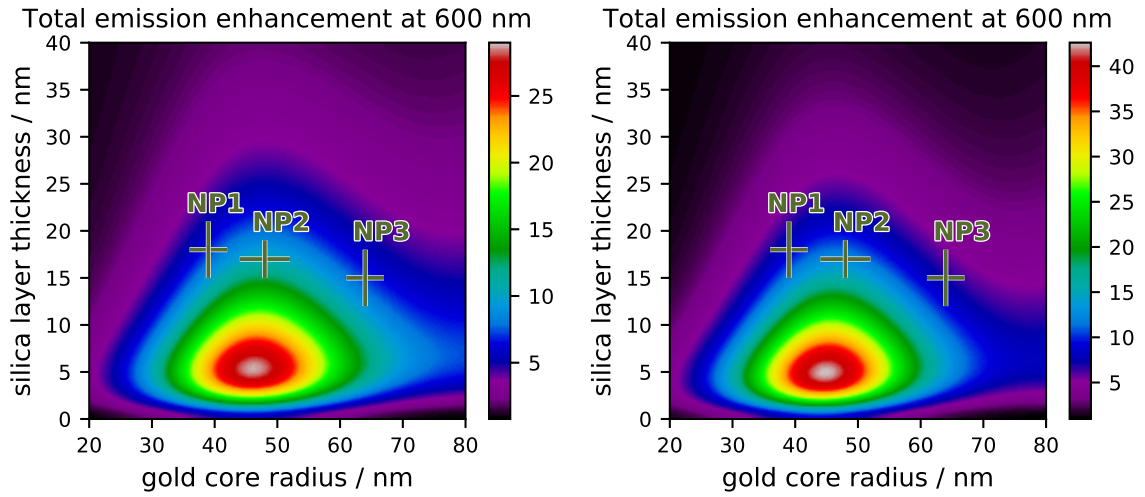

Figure S12: Simulated enhancement of the apparent brightness of the S_1 state emission for H_2TPP (left) and ZnTPP (right) excited at 600 nm attached to Au@SiO_2 nanoparticles of different core radii and silica shell thicknesses averaged over their respective emission spectra.

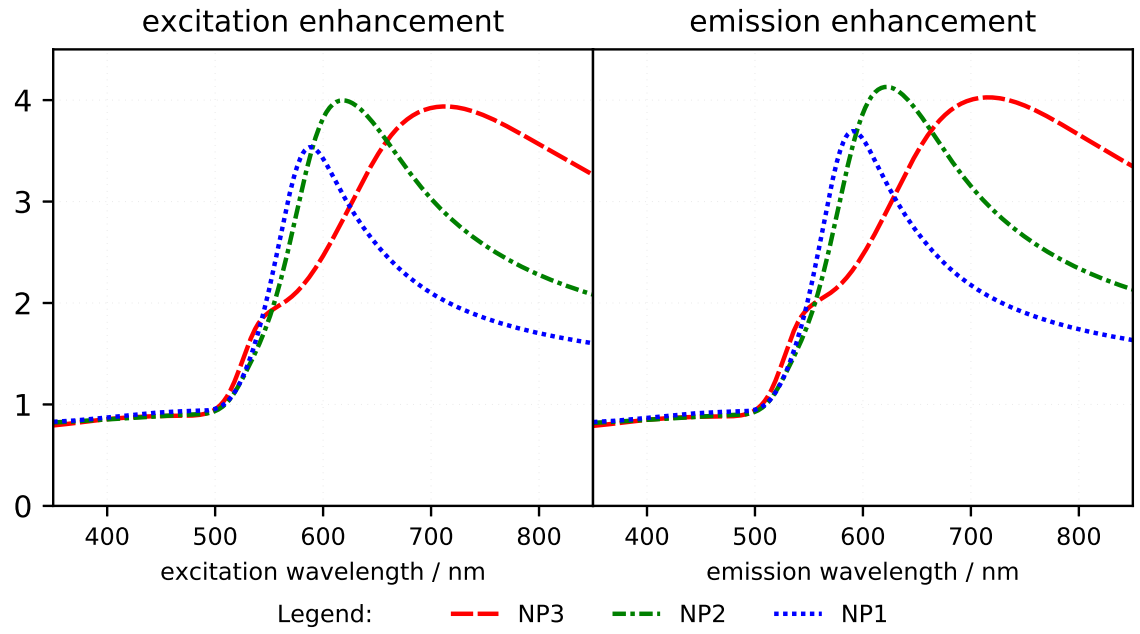

Figure S13: Simulated enhancement profiles for the excitation rate (left) and the radiative decay rate (right) calculated for the synthesized Au@SiO_2 nanoparticles.

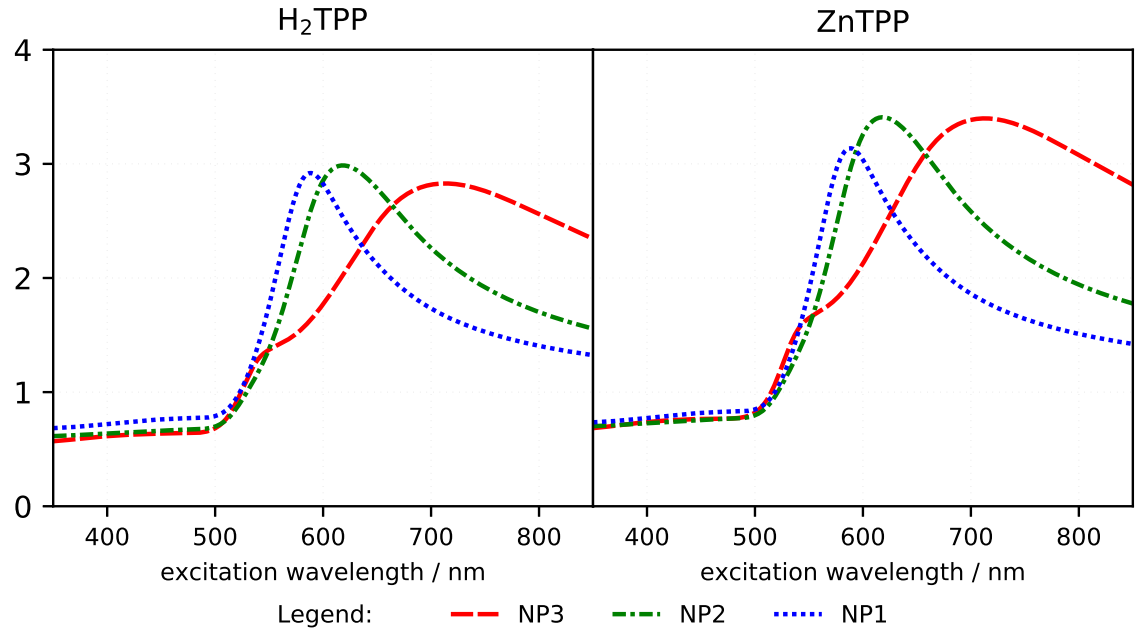

Figure S14: Simulated enhancement profiles for S_1 state population for H_2TPP (left) and ZnTPP (right) calculated for the synthesized Au@SiO_2 nanoparticles for different excitation wavelengths.

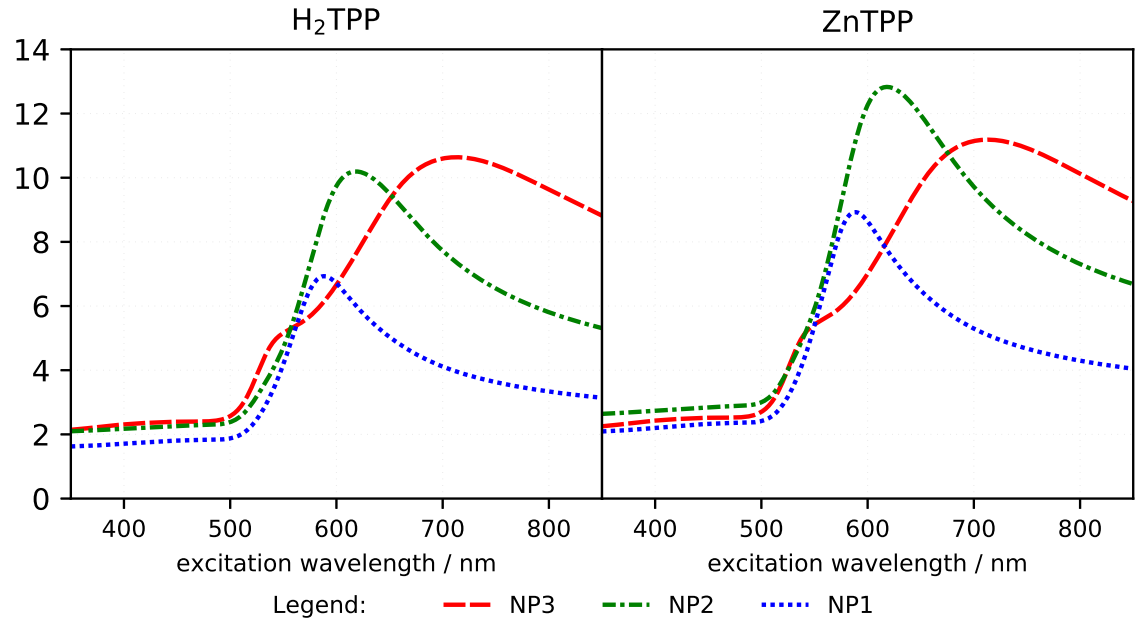

Figure S15: Simulated enhancement profiles for apparent emission brightness for H_2TPP (left) and ZnTPP (right) calculated for the synthesized $Au@SiO_2$ nanoparticles for different excitation wavelengths.

4. SEM

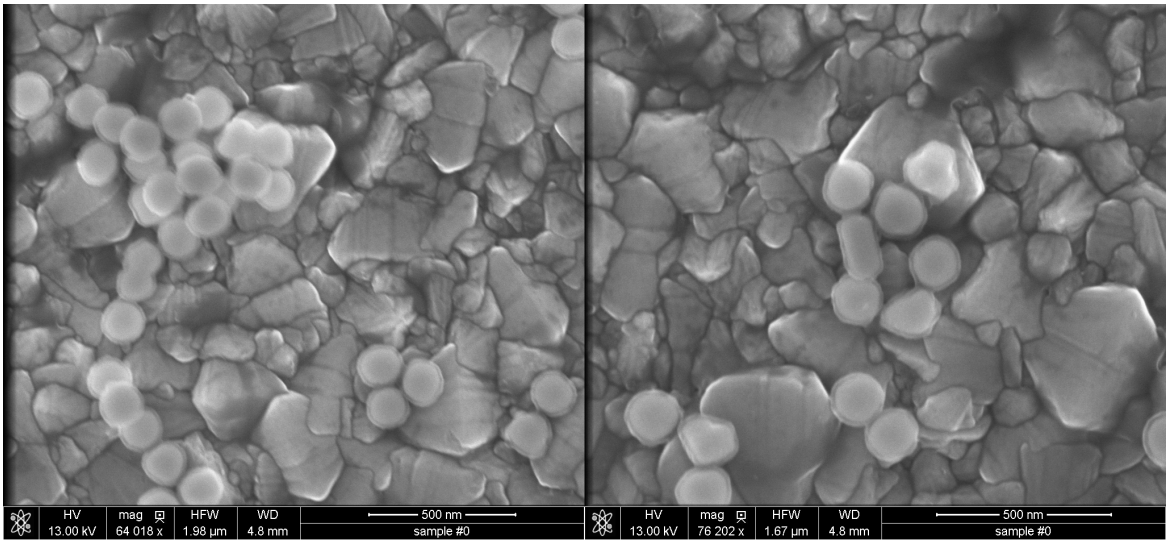

Figure S16: SEM images of NP3 nanoparticles.

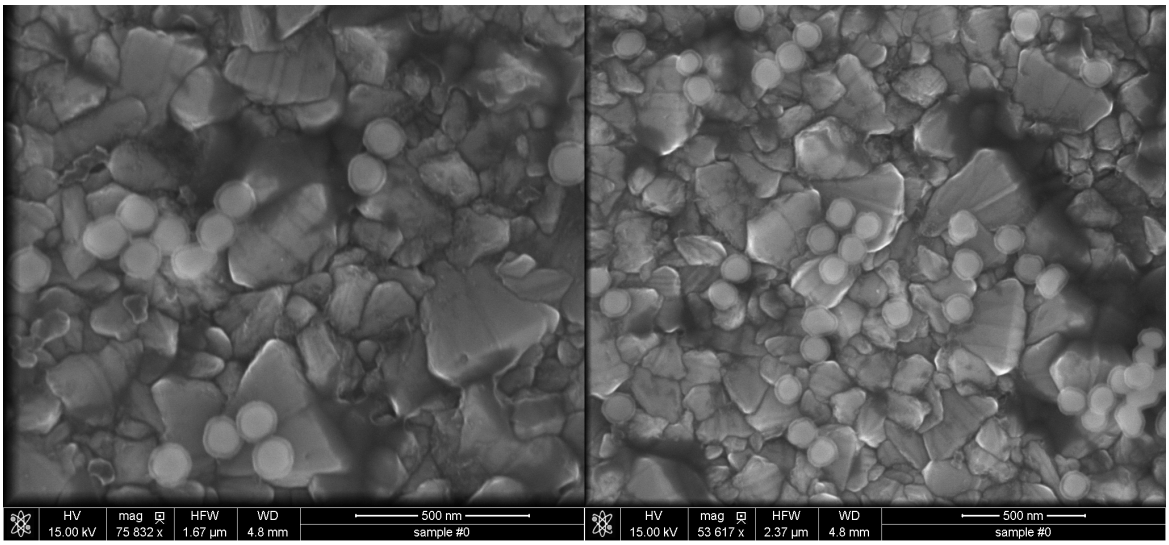

Figure S17: SEM images of NP2 nanoparticles.

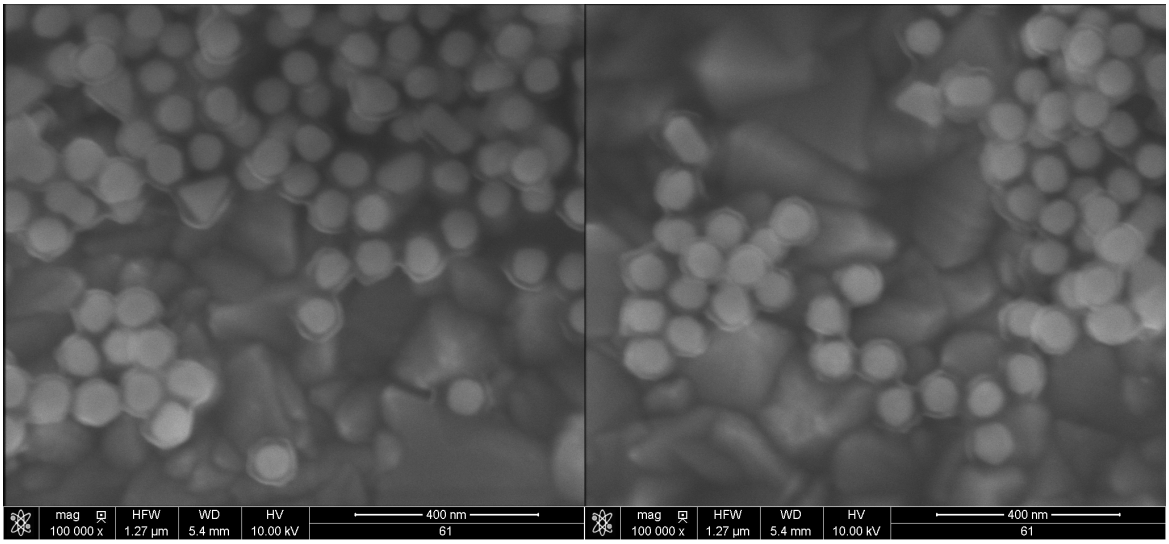

Figure S18: SEM images of NP1 nanoparticles.

5. ~~Extinction spectra~~

~~Experimental and simulated (Mie theory) extinction spectra of the Au@SiO_2 nanoparticles.~~

5. H_2TPP and ZnTPP photophysics before and after attachment to SiO_2 nanoparticles

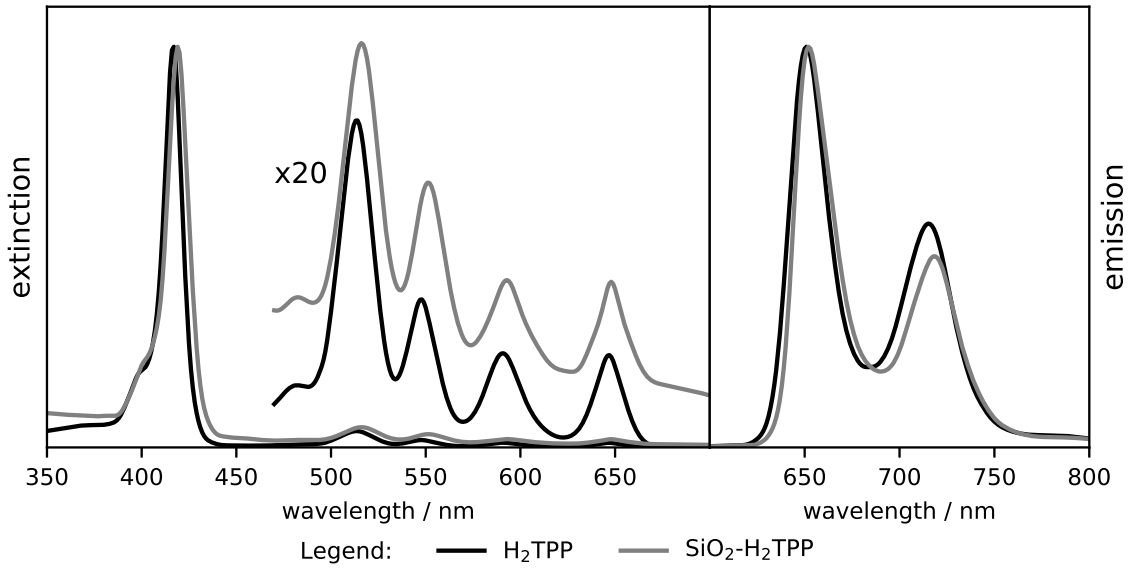

Figure S19: Extinction and emission spectra (excited at approx. 420 nm) of H_2TPP before and after attachment to SiO_2 nanoparticles.

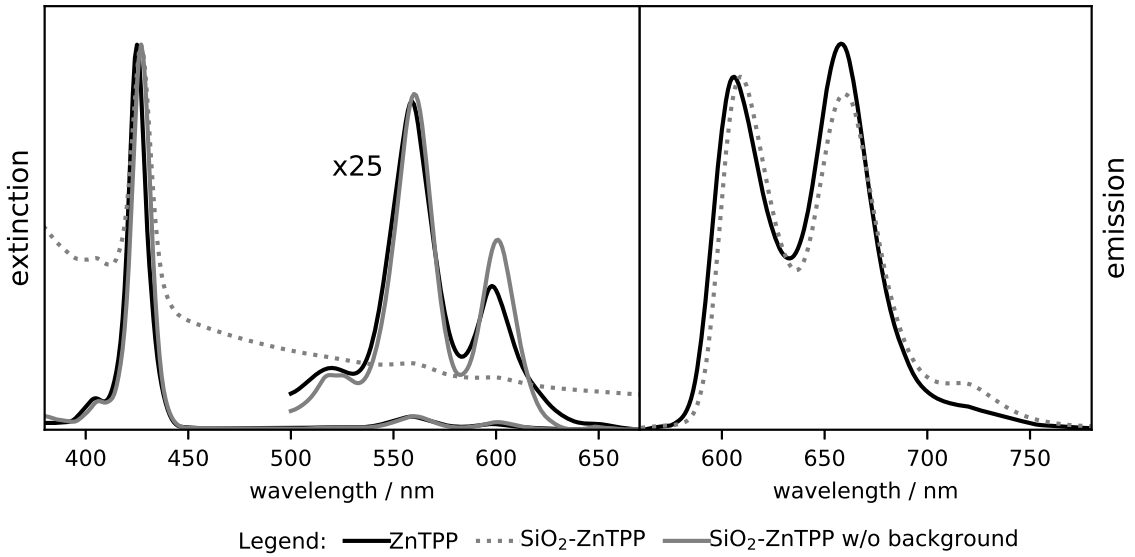

Figure S20: Extinction and emission spectra (excited at approx. 420 nm) of ZnTPP before and after attachment to SiO_2 nanoparticles. The gray curve in the left sub-figure shows the extinction spectrum after removal of scattering background. A small band in SiO_2-ZnTPP emission spectrum at around 725 nm results from the small fractions of remains of uncomplexed SiO_2-H_2TPP.

6. TCSPC decay curves and fitting

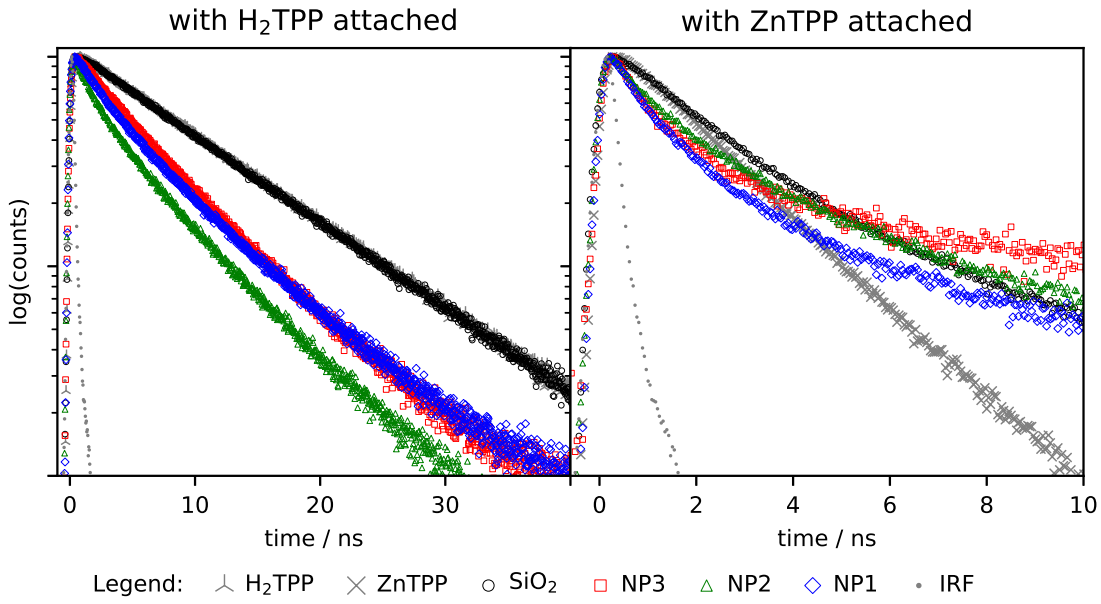

Figure S21: TCSPC emission decay curves for the functionalized nanoparticles and parent chromophores.

Table S1: Results of fitting of TCSPC decay curves for H_2TPP ~~and ZnTPP~~ before and after attachment to SiO_2 nanoparticles. The low amplitude short-lifetime components (2-3 ns) can possibly be attributed to protonated porphyrin aggregates [9–11]. The approx. 0.1 ns components are experimental artifacts.

	τ_1 / ns	A_1	τ_2 / ns	A_3	τ_3 / ns	A_3	χ^2_{red}
H_2TPP	10.462	1.000					1.325
SiO_2-H_2TPP	10.398	1.000					1.263
NP3-H_2TPP	7.951	0.847	1.892	0.132	0.085	0.021	1.661
NP2-H_2TPP	8.133	0.908	2.693	0.081	0.127	0.011	1.584
NP1-H_2TPP	8.243	0.789	2.689	0.197	0.105	0.014	1.586

Table S2: Results of fitting of TCSPC decay curves for ~~H_2TPP and~~ ZnTPP before and after attachment to SiO_2 nanoparticles. The low amplitude short time components (below 0.2 ns) are most probably experimental artifacts. Longer lifetimes (above 7 ns) result from parasitic silica defects luminescence [12–16].

	τ_1 / ns	A_1	τ_2 / ns	A_3	τ_3 / ns	A_3	χ^2_{red}
ZnTPP	1.87	0.43	0.07	0.57			1.455
SiO_2-ZnTPP	7.777	0.398	1.923	0.571	0.042	0.031	1.411
NP3-ZnTPP	21.631	0.703	1.441	0.21	0.006	0.087	1.271
NP2-ZnTPP	7.744	0.568	1.627	0.357	0.0171	0.0075	1.476
NP1-ZnTPP	10.36	0.469	1.656	0.379	0.119	0.152	1.551

References

[1] Jonathan S Lindsey and Richard W Wagner. Investigation of the synthesis of ortho-substituted tetraphenylporphyrins. *J Org Chem*, 54(4):828–836, 1989.

[2] Raymond J Abraham, Geoffrey R Bedford, David McNeillie, and Brian Wright. The NMR spectra of the porphyrins 16 - zinc (II) meso-tetraphenylporphyrin (Zn TPP) as a diamagnetic shift reagent. a quantitative ring current model. *Org Magn Reson*, 14(5):418–425, 1980.

[3] Gulimire Tuerdi, Patima Nizamidin, Nuerguli Kari, Abliz Yimit, and Fu Wang. Optochemical properties of gas-phase protonated tetraphenylporphyrin investigated using an optical waveguide NH_3 sensor. *RSC Advances*, 8(10):5614–5621, 2018.

[4] Cristina Fernández-López, Cintia Mateo-Mateo, Ramón A Alvarez-Puebla, Jorge Pérez-Juste, Isabel Pastoriza-Santos, and Luis M Liz-Marzán. Highly controlled silica coating of PEG-capped metal nanoparticles and preparation of SERS-encoded particles. *Langmuir*, 25(24):13894–13899, 2009.

[5] Jakub Ostapko, Joanna Buczyńska, Maria Pszona, Patrycja Kowalska, and Jacek Waluk. Synthesis, spectroscopy, and photophysics of porphyrins attached to gold nanoparticles via one or two linkers. *J Porphyr Phthalocyanines*, 18(08n09):686–697, 2014.

[6] Andreas M. Kern, Alfred J. Meixner, and Olivier J. F. Martin. Molecule-dependent plasmonic enhancement of fluorescence and Raman scattering near realistic nanostructures. *ACS Nano*, 6(11):9828–9836, 2012. PMID: 23020510.

[7] Maria C DeRosa and Robert J Crutchley. Photosensitized singlet oxygen and its applications. *Coord. Chem. Rev.*, 233:351–371, 2002.

[8] Reinhard Schmidt and Marcus Bodesheim. Collision-induced radiative transitions $b^1\Sigma_g^+ \rightarrow a^1\Delta_g$, $b^1\Sigma_g^+ \rightarrow X^3\Sigma_g^-$ and $a^1\Delta_g \rightarrow X^3\Sigma_g^-$ of O_2. *J Phys Chem*, 99(43):15919–15924, 1995.

[9] Pablo J. Goncalves, Daniel S. Correa, Paulo L. Franzen, Leonardo De Boni, Luciane M. de Almeida, Cleber R. Mendonca, Iouri E. Borissevitch, and Sergio C. Zilio. Effect of interaction with micelles on the excited-state optical properties of zinc porphyrins and J-aggregates formation. *Spectrochim. Acta, Part A*, 112:309–317, 2013.

[10] Maria Angela Castriciano, Andrea Romeo, Valentina Villari, Norberto Micali, and Luigi Monsù Scolaro. Nanosized porphyrin J-aggregates in water/AOT/decane microemulsions. *J. Phys. Chem. B*, 108(26):9054–9059, 2004.

[11] Maria Angela Castriciano, Andrea Romeo, Valentina Villari, Nicola Angelini, Norberto Micali, and Luigi Monsù Scolaro. Aggregation behavior of tetrakis (4-sulfonatophenyl) porphyrin in AOT/water/decane microemulsions. *J. Phys. Chem. B*, 109(24):12086–12092, 2005.

[12] Yuri D Glinka, Sheng-Hsien Lin, and Yit-Tsong Chen. Time-resolved photoluminescence study of silica nanoparticles as compared to bulk type-iii fused silica. *Phys. Rev. B*, 66(3):035404, 2002.

[13] Deyan Kong, Cuimiao Zhang, Zhenhe Xu, Guogang Li, Zhiyao Hou, and Jun Lin. Tunable photoluminescence in monodisperse silica spheres. *J Colloid Interface Sci*, 352(2):278–284, 2010.

[14] Lavinia Vaccaro, Adriana Morana, Viktor Radzig, and Marco Cannas. Bright visible luminescence in silica nanoparticles. *J. Phys. Chem. C*, 115(40):19476–19481, 2011.

[15] Lavinia Vaccaro, Luisa Spallino, Simonpietro Agnello, Gianpiero Buscarino, and Marco Cannas. Defect-related visible luminescence of silica nanoparticles. *Phys. Status Solidi C*, 10(4):658–661, 2013.

[16] Luisa Spallino, Lavinia Vaccaro, Luisa Sciortino, Simonpietro Agnello, Gianpiero Buscarino, Marco Cannas, and Franco Mario Gelardi. Visible-ultraviolet vibronic emission of silica nanoparticles. *Phys. Chem. Chem. Phys.*, 16(40):22028–22034, 2014.